

Short Communication

Preliminary ERS-1 Observations of Alaskan and Aleutian Volcanoes

Scott K. Rowland,^{*,†} Gregory A. Smith,^{*} and Peter J. Mouginis-Mark^{*,†}

We used ERS-1 radar images collected between October 1991 and February 1993 to study volcanic landforms of the Alaska Peninsula and Aleutian Islands. These data were used to map a little-eroded even-textured unit that is a thick low-mobility pyroclastic deposit around Aniakchak caldera. Also we have identified possible caldera remnants at Black Peak, and located volcanically related collapse pits and depressions in the summit glacier of Veniaminof. Observations of Westdahl and Mt. Spurr, both of which erupted during our observation period, demonstrate that new lava flows and debris flows can be mapped by virtue of their high radar backscatter and contrast with the surrounding terrain. These data demonstrate the utility of frequent orbital radar observations in this area. Regional mapping can be carried out for volcanoes that are difficult to study in the field due to adverse working conditions (e.g., frequent cloud cover, bad weather, long periods of darkness during winter) and remote locations; timely acquisition of images soon after or during an eruption can assist in the monitoring of active volcanoes. The 23° incidence angle causes strong foreshortening, and there is sometimes up to 35 days between repeat observations of certain locations. However, we conclude that the routine collection of SAR data from ERS-1 can provide valuable rapid information for assessing volcanic hazards in this region whatever the weather or time of year. The situation will be improved with the additional use of JERS-1 data and the launch of the Radarsat spacecraft in 1995.

INTRODUCTION

With the launch of the ERS-1 (European Remote-sensing Satellite-1) spacecraft in July 1991 (Francis et

al., 1991), routine observations of large areas of the Earth's surface with active microwave sensors became a reality. Through data acquisitions made by the Alaska SAR Facility in Fairbanks, Alaska, volcanoes from north Kamchatka, through the Aleutians and Alaskan Peninsula, to the northern Cascades can be imaged (Fig. 1).

The Aleutian and Alaskan volcanoes form a concave-northward arc stretching some 2500 km from Buldir Island to Hayes volcano (Fig. 2). These volcanoes have been described both tectonically and petrologically as constituting a classic volcanic arc (e.g., Burk, 1965; Kay and Kay, 1982; Marsh, 1982; Wood and Kienle, 1990, and references therein). The arc comprises 80 volcanoes, of which 24 have calderas >5 km across (Wood and Kienle, 1990). There have been over 350 eruptions from 45 different volcanoes along the arc since the early 1700s (Simkin et al., 1981; McClelland et al., 1989).

Field work on the majority of these volcanoes is notoriously difficult due to their remote locations and the extreme climate (Byers, 1959; Wood and Kienle, 1990). Frequent cloud cover (among other unpleasant field conditions) and long periods of darkness during the winter make orbital radar observations an excellent method for both regional mapping and the rapid acquisition of new information during or soon after an eruption. In this preliminary analysis of the ERS-1 data, we demonstrate the value of orbital radar images in the large-scale geologic interpretation of three volcanoes (Aniakchak, Black Peak, and Veniaminof). Descriptions of the 1991-1992 eruption of Westdahl, and the 1992 eruptions of Mt. Spurr are also included to show how potentially hazardous eruptions could be investigated with single-frequency, single-polarization orbital radars such as ERS-1, JERS-1 (Japan Earth Resources Satellite-1), and other planned orbital radars such as the Canadian Radarsat missions will expand and improve this capability particularly because they will provide better viewing geometries (see below).

Our investigation also lays some of the groundwork for future satellite-based volcanology investigations to

^{*} Planetary Geosciences, Department of Geology and Geophysics, School of Ocean and Earth Science and Technology, Honolulu

[†] Hawaii Center for Volcanology

Address correspondence to Scott K. Rowland, Planetary Geosciences, Dept. of Geology & Geophysics, School of Ocean & Earth Science & Technology, 2525 Correa Rd., Honolulu, HI 96822.

Received 22 February 1993; revised 18 September 1993.

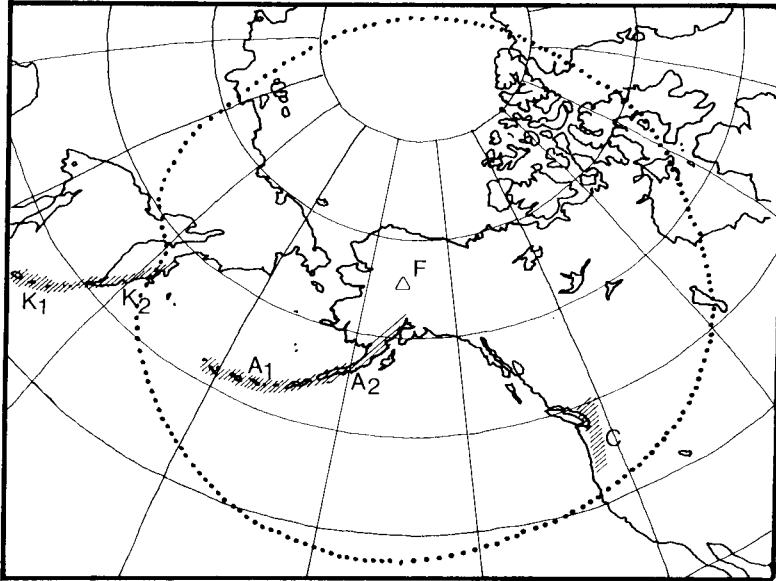


Figure 1. Location map showing the Alaska SAR Facility mask (dotted). Lined shading indicates locations of volcanic arcs: (K_1) Kurile Islands; (K_2) Kamchatka Peninsula; (A_1) Aleutian Islands; (A_2) Alaska Peninsula; (C) Cascades; (F) Fairbanks, location of Alaska SAR Facility (map modified from DeSoto et al., 1991).

be accomplished by the Earth Observing System (Mouginis-Mark et al., 1991; Mouginis-Mark and Francis, 1992). For this reason, we are in the process of obtaining images of all the Aleutian and Alaskan volcanoes as baseline data for later comparison after an eruption.

ERS-1 SENSOR CHARACTERISTICS

The ERS-1 spacecraft is in a sun-synchronous orbit (with an equatorial crossing time of 10:30 a.m.) at an altitude of 780 km. The spacecraft's payload (Francis et

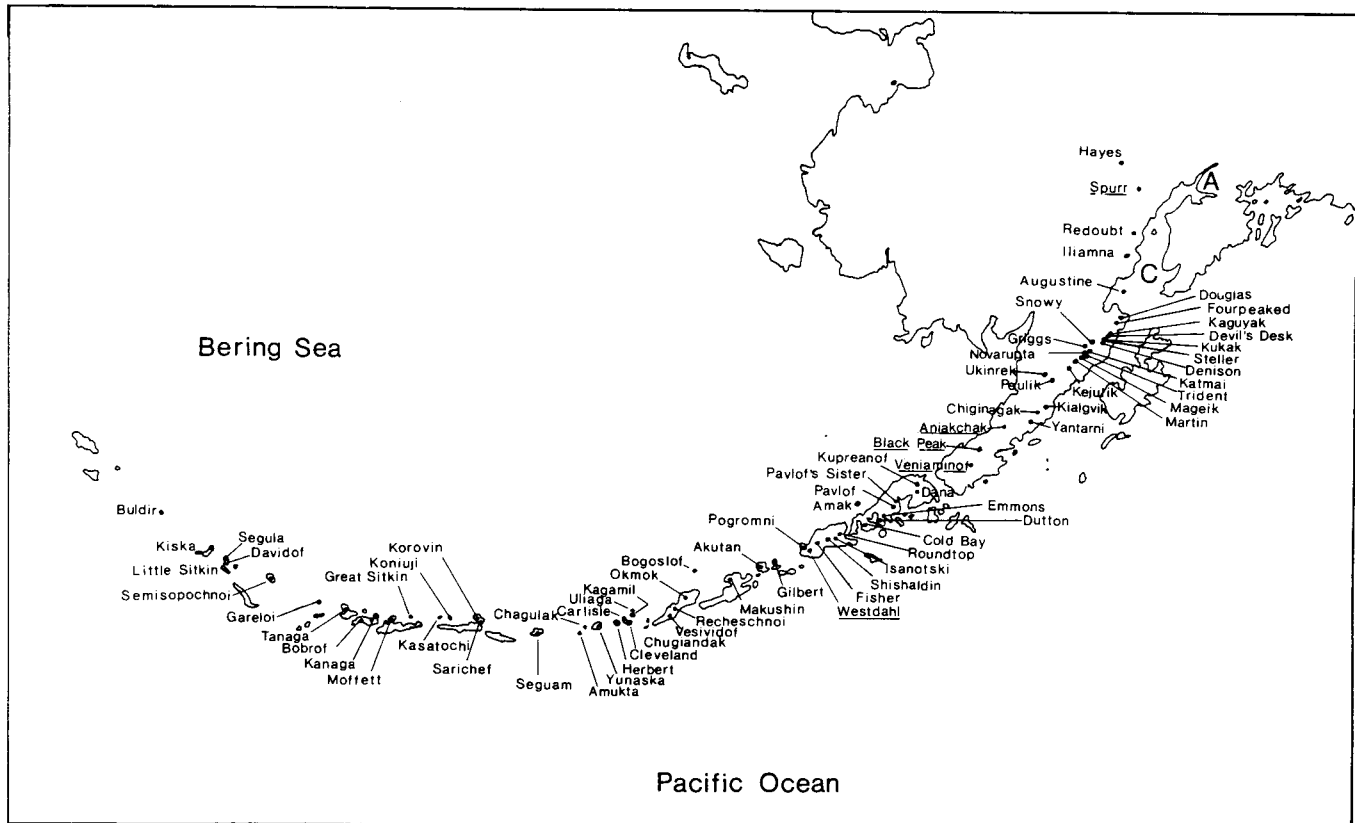


Figure 2. Map of the Aleutian and Alaskan volcanic arc showing the locations of Quaternary volcanoes (adapted from Stone, 1976; Wood and Kienle, 1990). Names of volcanoes discussed in text are *underlined*.

al., 1991) includes a VV-polarization, C-band (6 cm), synthetic aperture radar (SAR). The incidence angle along the center of the image swath is 23° and the spatial resolution is 30 m. Geometric correction by the Alaska SAR Facility produces good planimetric control, and in the process the data are resampled to 12.5 m. The swath width is about 100 km.

The ERS-1 orbit has been designed to maximize the scientific returns of several instruments in addition to the SAR (Bruzzi, 1991). For this reason two operating modes are used which dictate when SAR data can be obtained for a particular point on the ground. An ice mapping mode utilizes a 3-day orbit to allow frequent revisiting of areas of critical ice movement (such as the Baltic Sea and Gulf of Bothnia) between January and March each year. Multidisciplinary observations are made throughout the rest of the year using a 35-day repeat orbit mode. These two modes for the spacecraft mean that certain parts of Alaska and the Aleutians can be imaged with the same viewing geometry every 3 or 35 days, whereas during the 3-day repeat there are some targets that cannot be imaged at all. To date, after ~16 months of data acquisitions, we have succeeded in obtaining at least one ERS-1 image of 46 different volcanoes, and multiple images (both from ascending and descending orbits) of 10 of these.

The 23° incidence angle of the ERS-1 SAR was selected to facilitate many oceanography and sea ice investigations. This incidence angle produces pronounced foreshortening and layover when slopes of ~15° or more are imaged. This is not an insignificant problem when studying volcanoes, and for this reason, our study has, to date, concentrated mostly on the analysis of data covering the lower slopes of strato volcanoes and the relatively flat floors of calderas. JERS-1 and Radarsat have and will have higher incidence angles (35° and 20–55°, respectively), allowing a greater range of landforms to be studied.

MAPPING OF 3 LARGE CALDERAS

Aniakchak, Black Peak, and Veniaminof have been selected to show the value of synoptic mapping of volcanoes using the ERS-1 SAR data. These three volcanoes (Figs. 2 and 3) all produced large ash eruptions within the last 5000 years (Miller and Smith, 1987; Wood and Kienle, 1990). Calderas formed concurrent with the ash eruptions at Aniakchak and Veniaminof, and all three volcanoes present a variety of volcanic features, ages of surface units, and degrees of weathering. Although they have been mapped in detail (Detterman et al., 1981a,b), the ability of the ERS-1 SAR to accentuate subtle topographic features at the 1 to 10 km scale permits several large-scale structures and eruptive units to stand out for closer analysis.

Aniakchak

Aniakchak consists of an ice-free caldera ~10 km across (Figs. 3A and 4; Wood and Kienle, 1990; Neal et al., 1992). It is a good example of the numerous caldera-possessing volcanoes in the Aleutian–Alaskan arc. Associated with caldera formation was the emplacement of extensive highly mobile pyroclastic flows that reached both the Bering Sea and Pacific Ocean coasts (Miller and Smith, 1977). Postcaldera eruptions have formed numerous vent constructs including tuff cones and a 1000-m-high cinder / spatter cone called Vent Mountain, as well as thick dacite lava flows (Wood and Kienle, 1990; Neal et al., 1992).

About 10 km from the caldera rim, a break in slope within the relatively uneroded northwest sector of the volcano shows up prominently in the ERS-1 image. Although present in the topographic maps (but undistinguished in the geologic maps), this feature is enhanced and made obvious in the radar image. This break in slope appears to be the outer edge of a relatively thick unit that underlies the more extensive pyroclastic falls and flows. We suggest that it is a proximal low-mobility deposit that either erupted on the northwest side of the volcano or was directed towards the northwest. This deposit is ~140 km² in area. The preferential distribution of the deposit suggests that there may have been a high southeast caldera wall already in existence that prevented its flowing in that direction (the later high-mobility flows would not have noticed this boundary). Tom Miller (pers. commun., 1992) confirms that this unit consists of thick relatively welded agglutinate from an early phase of the caldera-forming eruption. He suggests that it is only on the northwest sector because it erupted from an arcuate fissure on this side of the volcano prior to collapse of the main edifice. It was this main edifice that provided the topographic barrier preventing deposition to the southeast.

Regardless of the exact origin of this thick unit, its uneven distribution has resulted in the striking erosional asymmetry at Aniakchak. The northwest flanks were presumably as eroded as those to the southeast at the time of the eruption; however, they have been deeply buried and only slightly incised since then. The 23° incidence angle of the radar caused this subtle unit to become obvious on the relatively featureless northwest flank of Aniakchak. The unit was buried by the thinner high-mobility pyroclastic flows and crops out only in a few gullies (T. Miller, pers. commun., 1992). Thus the radar has been able to accentuate a thick and extensive (but poorly exposed) unit that provides information on the events accompanying the caldera-generating eruption.

Within the caldera, Vent Mountain is prominent, as are a number of smaller pyroclastic cones. Additionally, there are a number of stubby, thick-looking radar-bright

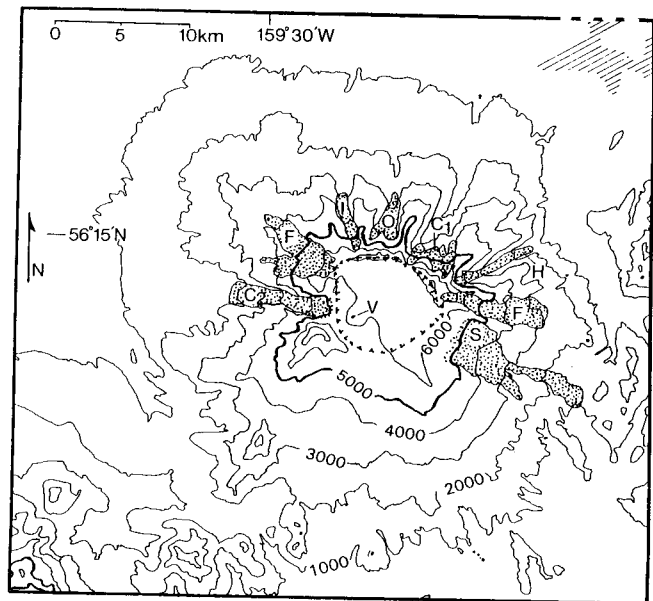
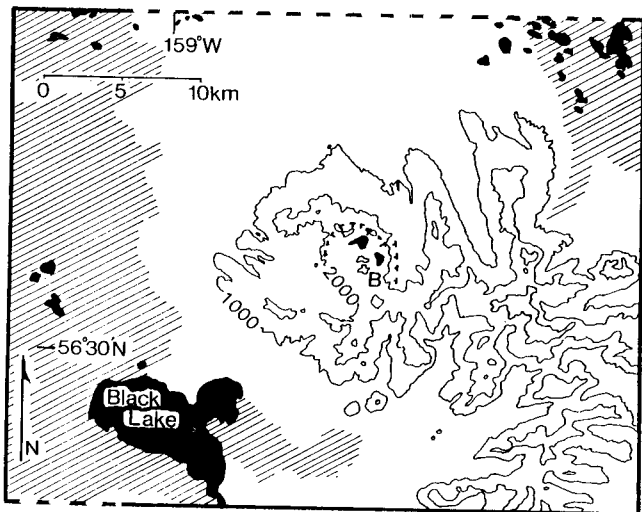
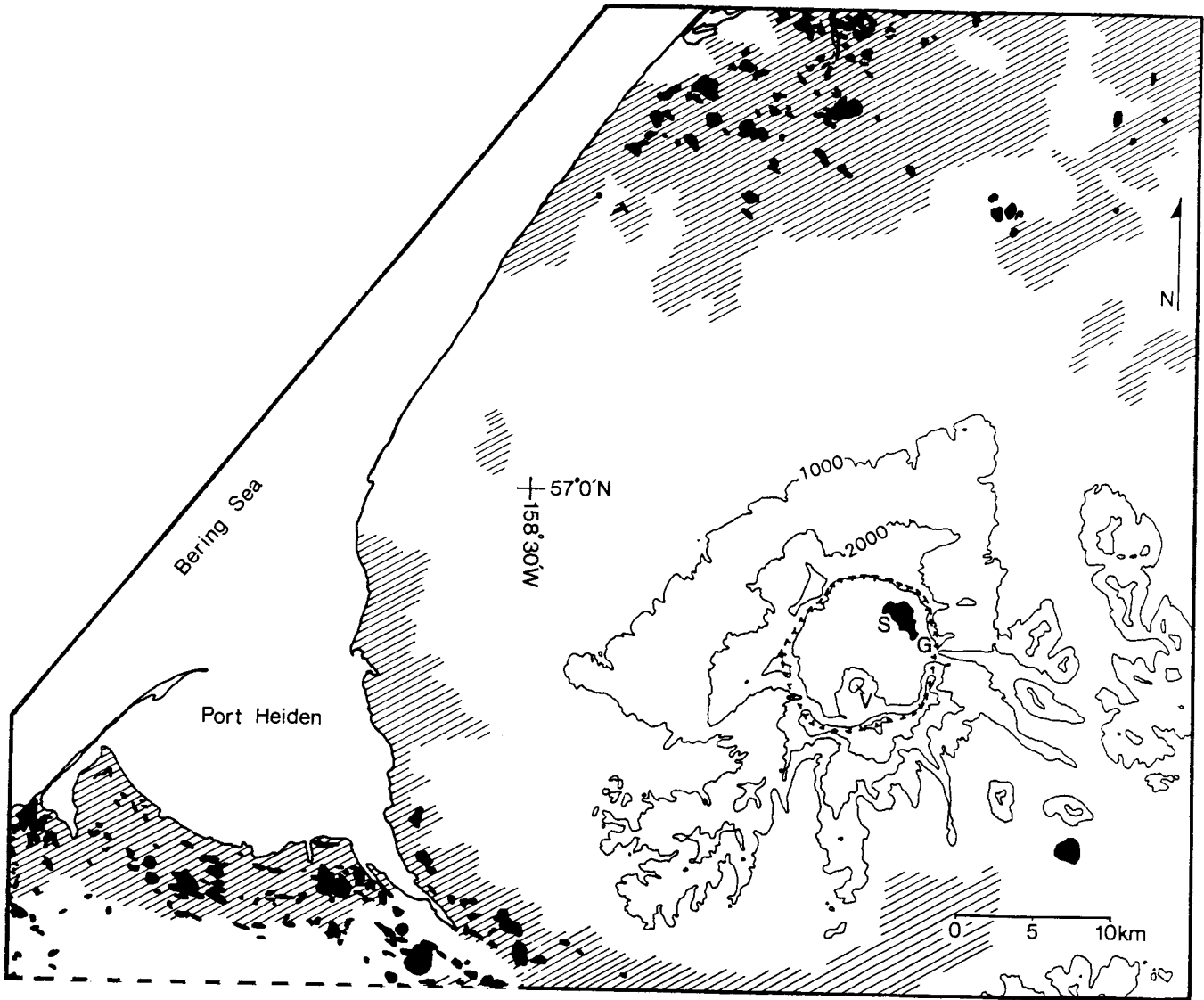




Figure 4. Aniakchak image (©ESA 1992). Vent Mtn. (V) and Surprise Lake (S) are labeled. Postcaldera features include several cinder cones (C) and lava flows (L), and except for one flow to the northeast are confined to the caldera floor. The low-mobility pyroclastic unit makes up the northwest sector of the volcano, and it is conspicuous by its lack of dissection. It appears to have been emplaced in two lobes around a preexisting topographic high that is elongated in a northwest direction. A faint radar-bright line (arrows) in the east caldera wall may correspond to the top of the underlying Jurassic rocks. Scale bar is 10 km.

flows. These are all, of course, postcaldera features, and in total they number about 10. This yields an average rate of one intracaldera eruption every 340 years in the time since the caldera formed 3400 years ago (Miller and Smith, 1977; 1987). There do not appear to be any postcaldera-formation features outside the caldera except for a truncated lava flow to the northeast (and its vent was in the caldera). The most recent activity was in 1931 (Simkin et al., 1981; Wood and Kienle, 1990).

The caldera collapsed into the underlying Jurassic basement, which is exposed about halfway up the eastern wall (Detterman, 1981a,b). An irregular radar-bright line subparallel to the caldera floor and rim can barely be distinguished and may be this boundary, made obvious by differential erosion.

Black Peak

Black Peak consists of a dome complex / strato volcano (Wood and Kienle, 1990) with a small caldera (Fig. 3B).

Figure 3. Location maps of three calderas. Contours are in feet, caldera outlines are indicated by dashed hachures, standing water is black, and swamps are indicated by diagonal lines. The three maps adjoin each other, the dashed margins indicate the common boundaries. (Traced from U.S. Geol. Surv. 1:250,000 Chignik, Bristol Bay, Ugashik, and Sutwik Island quadrangles.) A) Aniakchak: The caldera rim is higher to the northwest, and the outer margin of the thick agglutinate unit (see text) roughly corresponds to the 1000-ft contour to the north and northwest. Vent Mountain [V; elev. 3350 ft (1021 m), and 1000 m above the caldera floor], and Surprise Lake [S; drained through The Gates (G) by the Aniakchak River], are the main features of the caldera. B) Black Peak: The highest point on Black Peak (B), is on one of the young domes and has an elevation of 3385 ft (1032 m). Two small lakes occupy low areas between the young domes. The rugged terrain to the east comprises the arcuate ridges; however, they are more obvious in the radar image (Fig. 5). C) Veniaminof: An unnamed cinder cone [V; elev. 7075 ft (2157 m)] has been the locus of all recent activity. The north rim of the caldera is higher and this flank of the volcano has numerous valley glaciers (stippled). Clockwise from the west, their names are Cone (C₂), Fog (F), Island (I), Outlet (O), Crab (C₁), Harpoon (H), Finger (F), and Slim (S). The south caldera rim is buried by snow and ice, as are the upper flanks of the volcano in this direction. Potential jokulhlaups flowing down this side of the volcano could threaten the town of Perryville (J. Kienle, pers. commun., 1993).

Black Peak is one of a number of Aleutian–Alaskan volcanoes that consist mostly of large domes within the avalanche caldera of an eroded volcanic complex. An ash probably associated with the formation of the large caldera is ~3600 years old (Miller and Smith, 1987; Wood and Kienle, 1990).

As can be seen in the ERS-1 image (Fig. 5), the youngest dome complex is a prominent feature. At least four domes or lobes can be seen within the arcuate-southward collapse structure. This collapse structure developed in a now-highly incised strato-volcano, which in turn is situated within one of a number of larger concave-westward ridges (see below). Just to the west northwest of the young domes is a thick relatively undissected unit. This may be an analog to the thick near-vent agglutinate on the northeast flank of Aniakchak, or it is itself another strato-volcano/dome complex. Similarly undissected deposits occur in two valleys on either side of the youngest dome complex, and they have been mapped as thick, low-mobility pyroclastic flows (Wood and Kienle, 1990).

One of the more striking features of the Black Peak image is the set of concave-west ridges to the east of the younger domes. There are at least four of these arcuate ridges spaced ~4 km apart and extending out to about 15 km from the youngest domes. The arcuate ridges are not particularly obvious in the topography (Fig. 3B) but show up prominently in the radar image; their orientation and curvature may be somewhat enhanced by the radar look direction. They have the form of nested avalanche calderas similar to those of Piton de la Fournaise (Duffield et al., 1982) and Colima (Robin et al., 1987). If analogous to those examples,

they indicate a younging of volcanic activity towards the west. Tom Miller (pers. commun., 1992) suggests that the young domes represent the present location of a magmatic center that has migrated westward through time.

Veniaminof

Veniaminof is a classic strato-volcano with a 9-km wide summit caldera (Figs. 3C and 6). Unlike Aniakchak, the Veniaminof caldera is full of ice and snow. The caldera formed ~3700 years ago (Miller and Smith, 1987), about the same time as those of Black Peak and Aniakchak. A cinder cone protrudes 330 m above the ice in the east part of the caldera, and it has been the locus of eruptive activity since at least 1930 (Wood and Kienle, 1990). This cone is one of many on Veniaminof; they define a prominent northwest-southeast band across the volcano. The northwest flank of Veniaminof is blanketed by thick ash flow and fall deposits from the caldera collapse event (Detterman et al., 1981a,b).

Depressions and pits in the summit ice cap can be interpreted as evidence of eruptive activity. They form either when eruptions take place under the ice (melting a cavern and removing support from below), or when lava flows onto the ice surface. Pits were formed by both processes during the 1983–84 eruption of Veniaminof (Yount et al., 1985; McClelland et al., 1989). The largest of the 1983–84 pits is visible in the ERS-1 image just to the southeast of the main cone. It is about 1650 m across. Two smaller depressions are visible along the south margin of the caldera. These are much less distinct and are about 370 m and 200 m across. On an ice-covered volcano (of which there are many world-wide),

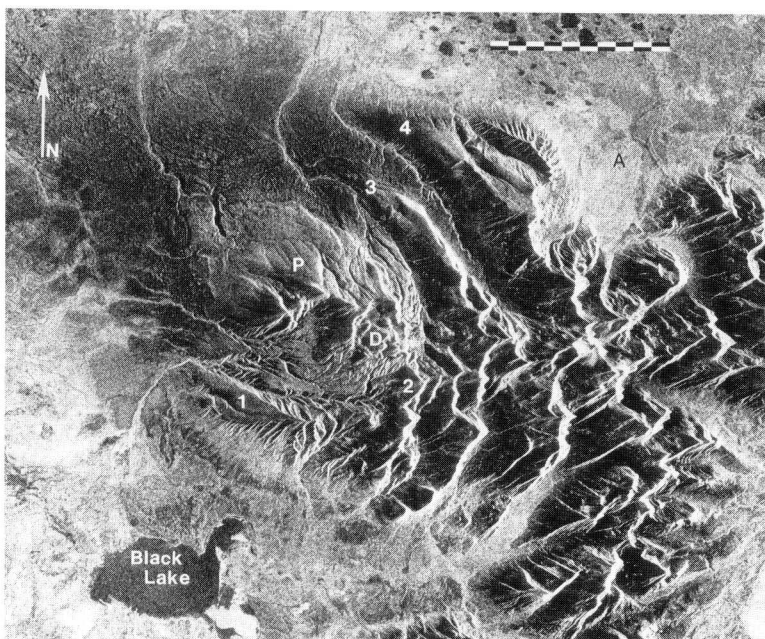


Figure 5. Black Peak image (^CESA 1992). The central dome complex (*D*) resides in a south-facing amphitheater, and four to five separate domes can be identified. To the northwest is a little-dissected unit of probable pyroclastic origin (*P*), possibly similar to that found at Aniakchak. The arcuate ridges stand out prominently and are numbered 1–4 towards the east. Note the large radar-bright debris avalanche (*A*) extending to the northeast from the easternmost ridge. Scale bar is 10 km.

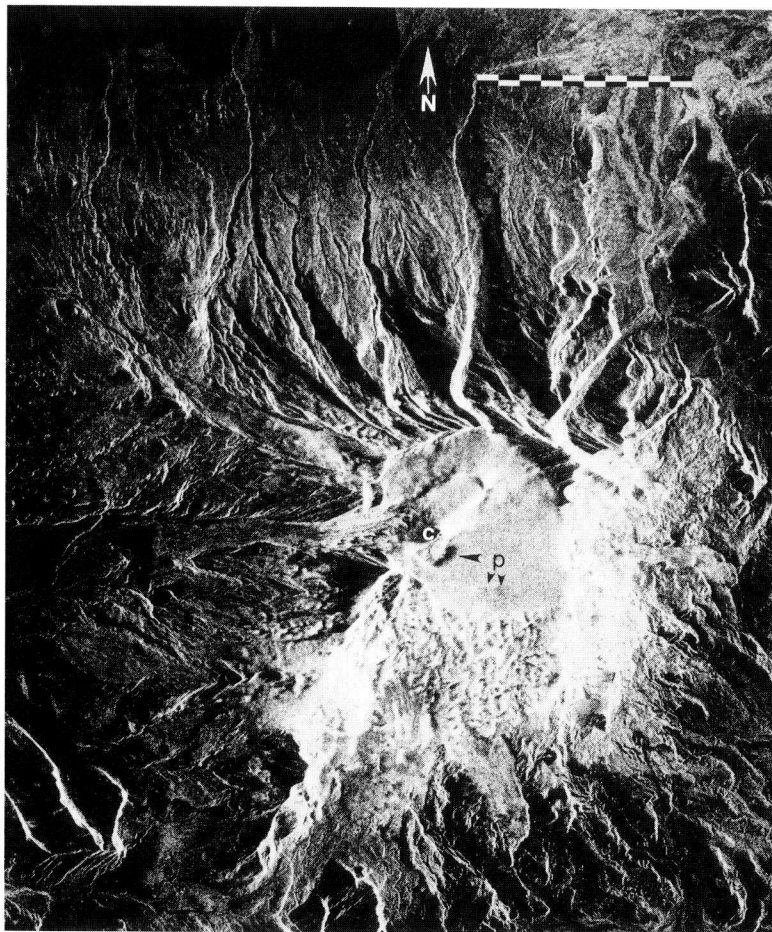


Figure 6. Veniaminof image ([©]ESA 1992). Three pits (*P*) in the permanent snow and ice cap of the summit can be seen. One of these is at the southeast base of the recently-active cone (*C*) and formed by melting and collapse during the eruption of 1983–84. Its edges have been somewhat muted by intervening snowfall. The lava that flowed from the cone into the pit makes up the radar-bright north-west half of the pit. The south margin of the caldera shows up as a texture change in the permanent snow cap. The two small additional pits just north of the south margin may have been formed by eruptions under the ice. Scale bar is 10 km.

such depressions in the ice may be the first indications of eruptive activity. The ability of the ERS-1 radar to accentuate the subtle topographic signature of these features makes it particularly useful in such cases. Jokulhlaups are a distinct hazard on an active volcano with an ice-filled caldera (Wood and Kienle, 1990). The pit melted in the ice cap during the 1983–84 eruption had a volume of $\sim 0.1 \text{ km}^3$ (Yount et al., 1985; McClelland et al., 1989); however, no jokulhlaups were recorded.

OBSERVATIONS OF RECENT ACTIVITY

A key attribute of orbital sensors is their ability to obtain new data of the Earth's surface during or soon after changes on the ground. In the case of volcanic eruptions, while the spatial resolution of the ERS-1 SAR will not replace measurements and observations made in the field, it is frequently impractical to organize at short notice a field expedition to a remote eruption site. Obtaining orbital images during the growth of a lava flow, or before and after scenes of an active summit crater, can be invaluable when planning subsequent field observations during or after an eruption. The synoptic view with good planimetric control is particularly

useful for determining the area of new volcanic deposits as long as they are not in areas of significant layover. During the first year of operation of the ERS-1 spacecraft, there were two eruptions that demonstrate the value of an orbital SAR. Westdahl began erupting on 29 November 1991, and continued until 15 January 1992. Mt. Spurr had a series of eruptions between June and September 1992. We present summaries of these two eruptions as viewed by ERS-1 in order to show how future eruptions might be studied by orbital radars.

The 1991–92 Westdahl Eruption

Westdahl volcano comprises the southwest end of Unimak island and is an ice-covered shield of mostly tholeiite basalt (Fig. 7; Wood and Kienle, 1990). Westdahl erupted in 1964 and 1978. Its most recent eruption in late 1991–92 provided an opportunity to study very young eruption features with ERS-1 data. Although the frequency of ERS-1 coverage was not sufficient to study temporal details of the eruption, the nature of the eruption was such that the new volcanic features can be easily identified. The following chronology comes from Bulletins of the Global Volcanism Network (GVN), Volume 16, Numbers 11 and 12, and Volume 17, Number

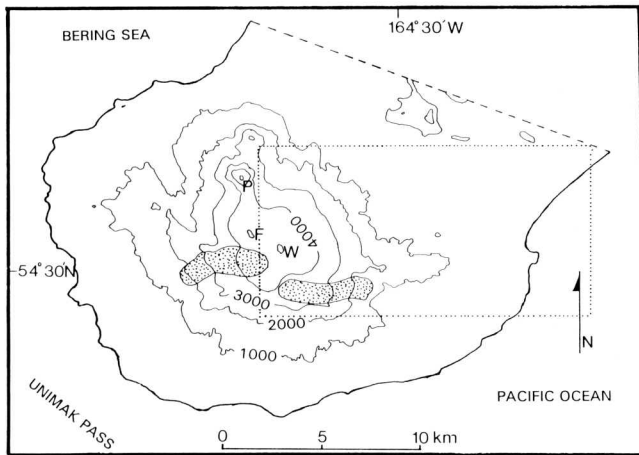


Figure 7. Map of the southwest end of Unimak Island, showing the location of Westdahl Volcano. Dotted box shows approximate outline of ERS-1 scene (Fig. 8). Contour interval 1000 ft, glaciers stippled. P, F, and W indicate the summits of Pogromni Volcano, Faris Peak, and Westdahl Peak at elevations of 2002 m, 1654 m, and 1560 m, respectively. Traced from U.S. Geol. Surv. 1:250,000 Unimak quad.

1. Westdahl began erupting at about 17:00 local time on 29 November 1991 from a fissure ~8 km long. The fissure extended from near Westdahl peak (the highest point on the volcano at 1560 m) eastward to an elevation of ~760 m. A dark-colored debris flow was emplaced to the Pacific coast, and a 5–10 m thick a'a flow advanced

4 km the first day. It was 7 km long by 30 November. The eruption continued until 15 January 1992 when a significant reduction in activity was recorded. After 3 December the flows did not advance much further but widened considerably.

Figure 8 is an ERS-1 image of Westdahl Volcano collected 27 February 1992, about a month after the last reported eruptive activity. The eruptive fissure of the 1991–92 eruption is visible, as are irregular canyons cut into the ice cap by lava and melt water. This canyon network opens out onto the middle slopes of the volcano.

The lava flow is radar-bright as is expected for a'a, and is indistinguishable in brightness from the 1964 flow. Air photographs (Fig. 9) taken in March 1992 differentiate them easily; the 1964 lava is snow-covered whereas the (still warm) 1991–92 lava is not. Additionally, the 1982 U.S. Geol. Surv. X-band radar map (Unimak sheet: map #54164-A1-RA-250-XO) shows the 1964 flow and allows for differentiation of the new lava. This is an excellent example of the value of baseline remote-sensing data.

The 1991–92 lava apparently flowed out from the fissure/canyon system and after spreading slightly entered narrow valleys on the lower slopes. The flow emerged from these valleys and coalesced on the floor of a much wider valley (formed between Westdahl and neighboring Fisher Volcano to the northeast) that drains to the Pacific coast. Lava reached 15.2 km from the west end of the eruptive fissure and covered an area of

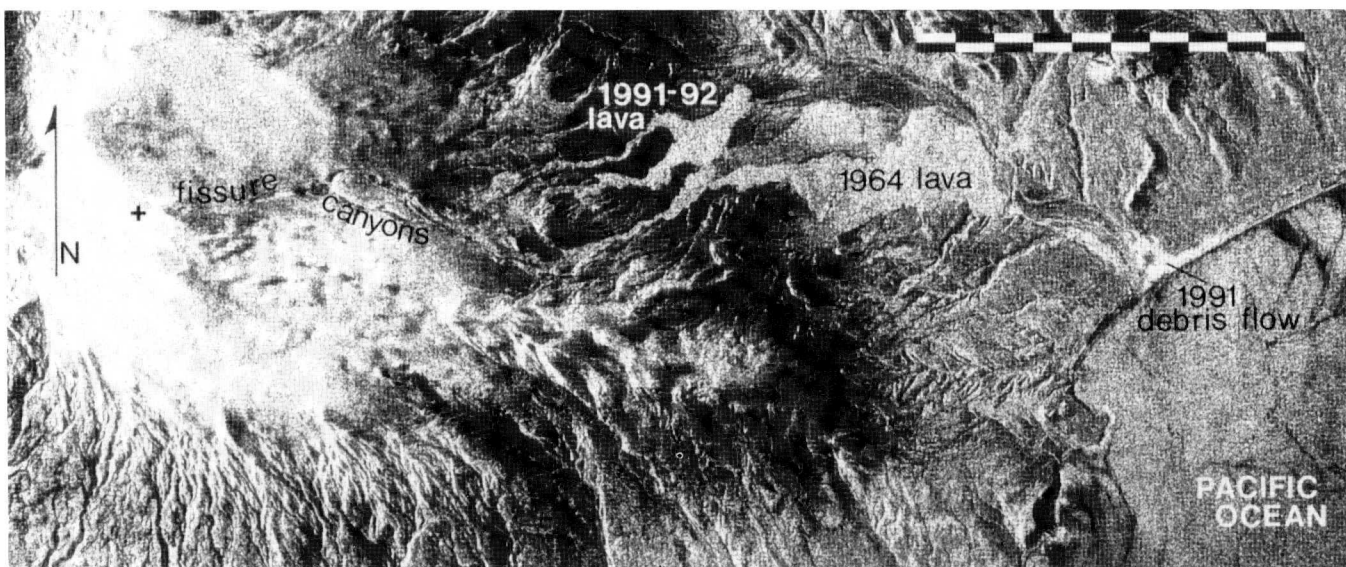


Figure 8. Westdahl image (ESA 1992). This image was acquired on 19 January 1992, shortly after the 1991–92 eruption ended. The main fissure is evident by a slightly lower radar brightness and by the central valley along its length. East of the fissure, irregular canyons have been cut into the snow and ice cap that covers the summit. After slight spreading, the lava entered valleys on the northeast flank, and in these traveled to the plain at the base of the volcano. Note that the 1991–92 flows are essentially indistinguishable from the 1964 flow. The debris flow deposit is confidently mapped only at its seaward end where it comprises the most radar-bright unit. Cross indicates Westdahl Peak (elev. 1560 m). Scale bar is 10 km.



Figure 9. Air photograph of Westdahl taken 13 February 1992 (U.S. Fish & Wildlife Service photo by Fred Zeille-maker, and kindly provided by T. Neal). The view is upflow towards the vent. Note the distinct differences in snow cover between the 1964 and 1991–1992 lavas. The foreground consists of the area over which the debris flow traveled.

6.3 km². The larger 1964 flow covered 12.7 km². Based on the report that the 1991 flow ceased advancing by 3 December, the average velocity was ~160 m/h. Using the reported thickness of 5–10 m, the total volume of 1991 lava is 0.03–0.06 km³, and if emplaced between 29 November and 15 January, yields an average volumetric flow rate of ~11 m³/s.

The distal end of the 1991 debris flow is easily distinguishable in the ERS-1 image; however, much of its upslope extent appears to have been buried by lava, and it left no radar-visible deposit where it flowed around the north margin of the 1964 lava. At the coastline, however, the debris flow is almost as radar-bright as the 1991–92 lava, reflecting its probable composition of boulders. It entered the ocean and apparently was redeposited by waves and currents along the coast.

The 1992 Eruptions of Mt. Spurr

Mt. Spurr is a steep-sided strato volcano located within the Tordillo Mountains, approximately 130 km west of Anchorage (Figs. 2 and 10). The volcano consists of an old andesite cone that has been breached to the south by an avalanche caldera (Wood and Kienle, 1990). The caldera is presently mostly ice-filled; Cone Peak, the only site of historic activity, protrudes through the ice. The following summary of activity comes from GVN Bulletin Volume 17, Numbers 5–8, and Alaska Volcano Observatory (1993). Beginning in August 1991, increased seismicity was recorded at Mt. Spurr centered under Cone Peak. Explosions from Cone Peak occurred on 27 June, sending an ash cloud 8 km high. Seismicity remained relatively high through July, and on 18 August a larger explosive eruption occurred; this time the eruption cloud went ~14 km high. A small pyroclastic flow

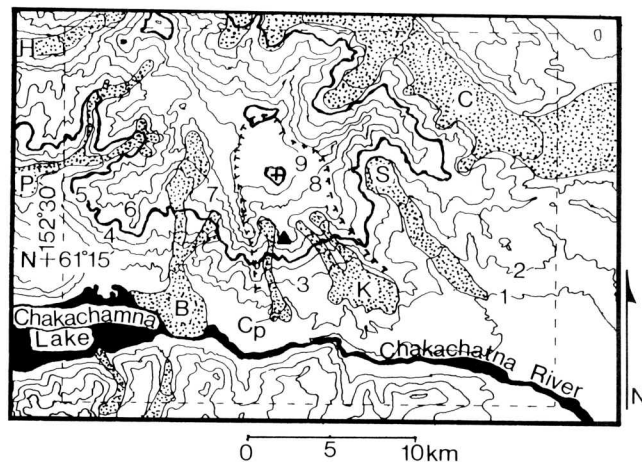


Figure 10. Location map for Mt. Spurr. Cross is Spurr Peak (3375 m), filled triangle ~4 km south is Crater Peak (2309 m), site of 1992 eruptions. Dashed hachured line indicates the shape of the avalanche caldera. Debris from this caldera has dammed the Chakachatna River to form Chakachamna Lake. Numerous glaciers (stippled) occur on the slopes of Mt. Spurr. They are the (clockwise from upper right) Capps (C), Straight (S), Kidzageni (K), Crater Peak (Cp), Barrier (B), Pothole (P), and Harpoon (H) glaciers. ERS-1 scenes (Fig. 11) are centered approximately on the Crater Peak vent. Contour interval is 1000 ft, with the 5000-ft and 10,000-ft lines slightly darker (numbers indicate elevations in thousand feet). Dashed box indicates area of Figure 11A. Traced from U.S.G.S. 1:250,000 Tyonek quad.

traveled from Crater Peak towards the south. Seismicity again remained high, and a third explosive eruption took place 16–17 September in two episodes separated by about an hour. The ash cloud reached 13–15 km altitude. Numerous small mud flows traveled down the south flank, and hot pyroclastic avalanches traveled down the east side of the cone and across the Kidzageni glacier. We have collected eight images of Mt. Spurr (e.g., Fig. 11), and their temporal relationship to the eruptive episodes is summarized in Table 1.

The general form of the volcano is marked on the preeruption (17 May) image (Fig. 11A). The collapse caldera faces south, and debris from the collapse has dammed the Chakachatna River to form Chakachamna Lake. The Kidzageni glacier is broad and fan-shaped, filling most of the breached slope. The 10 July image (Fig. 11B) shows no large-scale changes, consistent with the relatively small 27 June eruption. However, a radar-bright deposit can be seen to have flowed southwest from Crater Peak before making a turn south southeast, coming to rest with a broad flow front east of the Crater Peak Glacier. J. Eichelberger (pers. comm., 1992) confirms that this was a debris flow generated on 27 June. The 30 August image (Fig. 11C) is essentially unchanged from that of 12 July. The 27 June debris flow is again visible, but the pyroclastic flow generated during the

18 August eruption cannot be identified. The next image comes from 18 September (Fig. 11D), the day after the 16–17 September eruption. A radar-bright unit can be seen south of Crater Peak. Unlike the 27 June debris flow, this unit (probably a pyroclastic flow based on eruption reports) took a more direct southerly route. It came to rest covering the distal part of the 27 July debris flow. The most recent image shown is from 8 November (Fig. 11E). The debris flow and pyroclastic flow noted earlier are difficult if not impossible to identify. The flow was possibly buried by later (but not identifiable) deposits, or obscured by melting or disruption of the Kidzageni glacier onto which it was emplaced. One noticeable difference in the 8 November image is that on the north side of Cone Peak there are a number of gullies. These may have been caused by falling debris and/or melting snow.

Thus, ERS-1 SAR data were not especially useful for studying this particular eruptive sequence. This is due mainly to two factors: 1) the small size of the eruptions and their products and effects; and 2) the steepness of Mt. Spurr and the surrounding terrain. The use of a higher-incidence angle SAR (such as JERS-1 at 35°) would produce less distortion and make the identification of small-scale features and changes easier, particularly on the steeper strato volcanoes.

SUMMARY AND CONCLUSIONS

The ERS-1 radar data provide numerous views of volcanoes in one of the Earth's most active arcs. Regional mapping of the volcanoes, and the opportunity to obtain repeat coverage of active sites, provide important synoptic information that may not be easily obtainable on the ground because of weather, local logistics, or the size of the features. Our preliminary study shows the value of the ERS-1 data for updating geologic maps and providing an overview of on-going/recent eruptions. The 23° incidence angle of ERS-1 proves to be particularly useful for mapping subtle topographic features in featureless terrain such as the thick agglutinate layer underlying the extensive pyroclastic flows at Aniakchak and shallow depressions in the ice cap of Veniaminof. However, extensive foreshortening and layover in images of rugged terrain make analysis of steeper (>15°) volcanic slopes almost impossible. Incidence angles of ~35–50° would be more useful in certain situations, and these will indeed soon be available to the volcanological community (see below). In the case of the 1991–92 eruptions of Westdahl, the acquisition of radar images during the periods of poor light permitted the extent of lava flows and debris flows to be easily determined.

A key aspect in assessing the value of the radar data is the frequency of coverage of individual targets provided by the spacecraft. The availability of ERS-1 SAR data is a significant step forward in our ability to

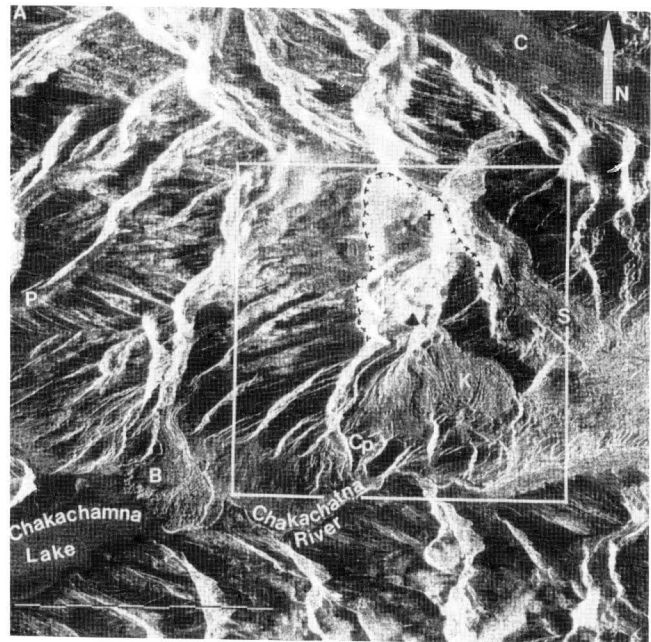


Figure 11. Five ERS-1 images of Mt. Spurr (^cESA 1992). A) Pre-eruptive image (17 May): the geographic features are marked as in Figure 10 (scale bar is 10 km; white box shows area covered by Figures 11B–E). B) 10 July image (following the eruption of 27 June): a debris flow (DF) is evident west of the Kidzageni glacier (K) C) 30 August image (following the eruption of 18 August): The earlier debris flow (DF) is still prominent but the pyroclastic flow generated during the 18 August eruption cannot be identified. D) 18 September image (following the 16–17 September eruptions): note the radar-bright pyroclastic flow (PF) that moved south from Cone Peak. The distal end of the earlier debris flow (DF) was buried by this pyroclastic flow. E) 8 November image: The earlier debris flow and pyroclastic flow are no longer evident; however, a number of gullies (G) can barely be made out on the north side of Crater Peak. Scale bar for Figures 11B–E is 5 km.

study Aleutian and Alaskan volcanoes. However, the fixed incidence angle and 3- or 35-day repeat orbits of the spacecraft do not permit each of the 80 potentially active volcanoes to be imaged as often as might be

Table 1. Activity and Collected Images of Mt. Spurr

<i>Mt. Spurr Activity</i>	<i>ERS-1 Scene</i>
Elevated seismicity since August, 1991	May 1 May 17 (Figure 11A) June 23 (JERS-1)
June 27 eruption	July 10 (2 scenes; Figure 11B)
August 18 eruption	August 30 (Figure 11C)
September 16–17 eruption	September 18 (Figure 11D) November 8 (Figure 11E)

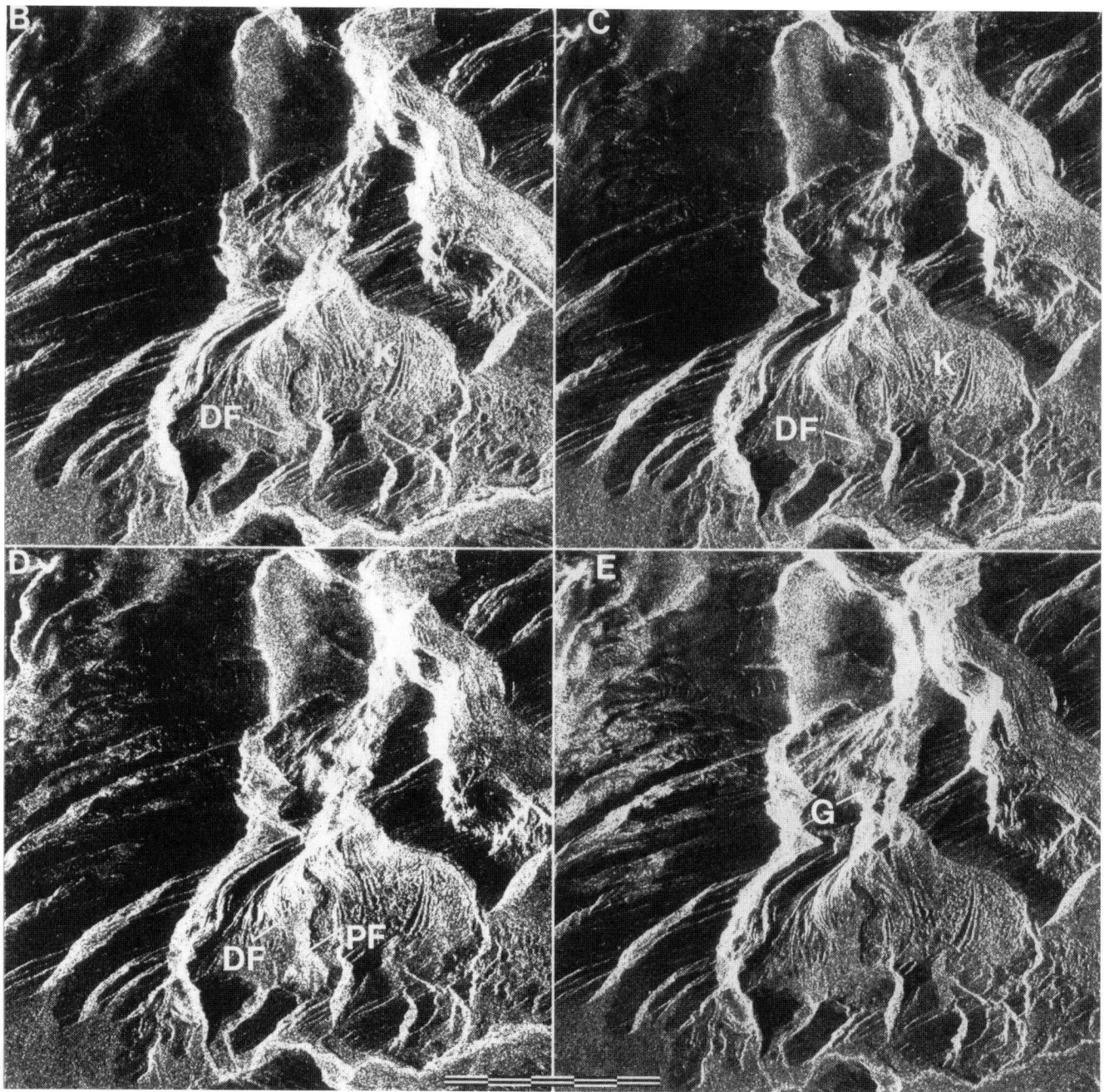


Figure 11. (continued)

desired. For example, it would be useful to obtain near-real-time radar images of volcanic eruptions that might be hazardous to aircraft since ingestion of volcanic ash by aircraft jet engines has been shown to be a very real hazard in this part of the world (Kienle et al., 1990; Kienle, 1991). A considerable amount of attention has recently been given to the automatic detection of eruption plumes using visible and infrared satellite data (e.g., Garbeil et al., 1993), but the detection of volcanic plumes requires their spectral discrimination from weather clouds. To our knowledge, no orbital radar

images have ever been obtained of an eruption plume, even though C-band data (such as these from ERS-1) might provide valuable insights into the structure and total ash content of the plume.

ERS-1 is the first in a series of orbital radars that should provide frequent images of erupting volcanoes. Images are also currently being obtained from JERS-1 radar, and Radarsat is planned for a 1995 launch. JERS-1, with an incidence angle of 35° , operates at L-band (23 cm) and has HH polarization, while Radarsat will be C-band (6 cm) HH polarization, and have a variable

incidence angle of 20–55°. These platforms should be followed by ERS-2 in 1996 and Envisat-1 in about 1998. Several of these radars should also be flying at any one time, thereby producing better temporal coverage of any particular site. Thus over the next few years there will be additional opportunities to study the temporal evolution of these volcanoes, as well as investigate the geomorphology of the steeper slopes of the volcanoes through the use of different incidence angle data.

We conducted no field work for this study so we are very grateful to Tina Neal, Tom Miller, and John Eichelberger of the Alaska Volcano Observatory for providing us with helpful comments regarding the detailed geology of these volcanoes. We also would like to thank Harold Garbeil, Karen Sender, and Lisa Petersen of SOEST for help in processing and printing the images, as well as Michelle Barr, Greta Reynolds, and Rose Watabe and the staff of the Alaska SAR Facility for providing both the images themselves, plus advice on how to process them. Two anonymous reviewers provided useful comments. This work was funded by Grant no. NAGW 2521 from the NASA Polar Programs Office of Mission to Planet Earth. This is SOEST Contribution No. 3492 and Planetary Geosciences Paper No. 746.

REFERENCES

- Alaska Volcano Observatory (1993), Mt. Spurr's 1992 eruptions, *EOS* 74:217–222.
- Bruzzi, S. (1991), The processing and exploitation of ERS-1 payload data, *ESA Bull.* 65:63–72.
- Burk, C. A. (1965), *Geology of the Alaska Peninsula Island Arc and Continental Margin*, Geol. Soc. Am. Mem. 99, 250 pp.
- Byers, F. M., Jr. (1959), Geology of Umnak and Bogoslof Islands, Aleutian Islands, Alaska, *U.S. Geol. Surv. Bull.* 1028-L:267–369.
- DeSoto, Y., Tippens, H., Kotlarek, T., and Hsu, L. (1991), *Alaska SAR Facility Archive and Catalog Subsystem User's Guide*, Jet Propulsion Laboratory Publication JPL D-5496, JPL, Pasadena, CA, 144 pp.
- Detterman, R. L., Miller, T. P., Yount, M. E., and Wilson, F. H. (1981a), Geologic map of the Chignik and Sutwik Island Quadrangles, Alaska, USGS Misc. Invest. Ser. Map I-1229.
- Detterman, R. L., Miller, T. P., Yount, M. E., and Wilson, F. H. (1981b), Quaternary Geologic map of the Chignik and Sutwik Island Quadrangles, Alaska, USGS Misc. Invest. Ser. Map I-1292.
- Duffield, W. A., Stieltjes, L., and Varet, J. (1982), Huge landslide blocks in the growth of Piton De La Fournaise, La Réunion, and Kilauea volcano, Hawaii, *J. Volcanol. Geotherm. Res.* 12:147–160.
- Francis, R., Graf, G., Edwards, P. G., et al. (1991), The ERS-1 spacecraft and its payload, *ESA Bull.* 65:27–48.
- Garbeil, H., Mouginiis-Mark, P. J., and Dean, K. G. (1993), Detection of eruption plumes from Redoubt Volcano using AVHRR images and multivariate analysis, *Remote Sens. Environ.*, forthcoming.
- Kay, S. M., and Kay, R. W. (1982), Tectonic controls on tholeiitic and calcalkaline magmatism in the Aleutian Arc, *J. Geophys. Res.* 87:4051–4072.
- Kienle, J. (1991), Volcanic ash-aircraft incidents in the years prior to the December 15, 1989 747 Redoubt encounter, in *First International Symposium on Volcanic ash and Aircraft Safety* (T. J. Casadevall, Ed.), U.S. Geol. Surv. Circ. 1065, U.S. Geological Survey, Washington, DC, pp. 27–28.
- Kienle, J., Dean, K.G., Garbeil, H., and Rose, W. I. (1990), Satellite surveillance of volcanic ash plumes, applications to aircraft safety, *EOS* 71:266.
- Marsh, B. D. (1982), The Aleutians, in *Andesites* (R. S. Thorpe, Ed.), Wiley, New York, pp. 99–114.
- McClelland, L., Simkin, T., Summers, M., Neilsen, E., and Stein, T. C. (1989), *Global Volcanism 1975–1985*, Prentice-Hall, Englewood Cliffs, N.J., 654 pp.
- Miller, T. P., and Smith, R. L. (1977), Spectacular mobility of ash flows around Aniakchak and Fisher calderas, Alaska, *Geology* 5:173–176.
- Miller, T. P., and Smith, R. L. (1987), Late Quaternary caldera-forming eruptions in the eastern Aleutian arc, Alaska, *Geology* 15:434–438.
- Mouginiis-Mark, P. J., and Francis, P. W. (1992), Satellite observations of active volcanoes: prospects for the 1990's. *Episodes* 15:46–55.
- Mouginiis-Mark, P., Rowland, S., Francis, P., Friedman, T., Garbeil, H., Gradie, J., Self, S., Wilson, L., Crisp, J., Glaze, L., Jones, K., Kahle, A., Pieri, D., Zebker, H., Krueger, A., Walter, L., Wood, C., Rose, W., Adams, J., and Wolff, R. (1991), Analysis of active volcanoes from the Earth Observing System. *Remote Sens. Environ.* 36:1–12.
- Neal, C. A., McGimsey, R. G., Braitseva, O., Miller, T. P., Eichelberger, J. C., and Nye, C. (1992), Post-caldera eruptive history of Aniakchak Caldera, Alaska, *EOS* 73(43):645.
- Robin, C., Mossand, P., Camus, G., Cantagrel, J. M., Gourgaund, A., and Vincent, P. M. (1987), Eruptive history of the Colima volcanic complex (Mexico), *J. Volcanol. Geotherm. Res.* 31:99–113.
- Simkin, T., Seibert, L., McClelland, L., Bridge, D., Newhall, C., and Latter, J. H. (1981), *Volcanoes of the World*, Hutchinson Ross, Stroudsburg, PA, 232 pp.
- Stone, D. B. (1976), Alaska's major volcanic centers (map), in *Alaska Geographic 4*, (R. A. Henning, C. H. Rosenthal, B. Olds, and E. Reading, Eds.), Alaska Northwest Publishing Company, Anchorage, p. 15.
- Wood, C. A., and Kienle, J. (1990), *Volcanoes of North America*, Cambridge Univ. Press, Cambridge, 354 pp.
- Yount, M. E., Miller, T. P., Emanuel, R. P., and Wilson, F. H. (1985), Eruption in an ice-filled caldera, Mount Veniaminof, Alaska Peninsula, in *USGS in Alaska: Accomplishments during 1983*, (S. Bertsch-Winkler and R. M. Reed, Eds.), U.S. Geol. Surv. Circ. 945, U.S. Geological Survey, Washington, DC, pp. 58–60.